Electronic Materials Letters, Vol. 9, No. 2 (2013), pp. 219-225
DOI: 10.1007/s13391-012-2142-7

Effect of Milling on Properties and Consolidation of TiO_2 by High-Frequency Induction Heated Sintering

In-Jin Shon,[1,*] Geon-Woo Lee,[1] Jung-Mann Doh,[2] and Jin-Kook Yoon[2]

[1]Division of Advanced Materials Engineering and the Research Center of Advanced Materials Development, Engineering College, Chonbuk National University, 561-756, Korea
[2]Interface Control Research Center, Korea Institute of Science and Technology, Seoul 130-650, Korea

(received date: 18 August 2012 / accepted date: 19 November 2012 / published date: March 2013)

Commercial TiO_2 powders were high-energy ball milled for various durations and consolidated using high-frequency induction heated sintering (HFIHS). The effect of milling on the sintering behavior, crystallite size and mechanical properties of TiO_2 powders were evaluated. A nanostructured dense TiO_2 compact with a relative density of up to 98% was readily obtained within 1 min. The ball milling effectively refined the crystallite structure of TiO_2 powders and facilitated the subsequent densification. The sinter-onset temperature was noticeably reduced by the prior milling for 10 h. Accordingly, the relative density of TiO_2 compact increased as the milling time increases. Furthermore, the microhardness and fracture toughness of sintered TiO_2 increased as the density increases. It is clearly demonstrated that a quick densification of nano-structured TiO_2 bulk materials to near theoretical density could be obtained by the combination of HFIHS and the preparatory high-energy ball milling processes.

Keywords: nanomaterials, sintering, hardness, fracture toughness, TiO_2

1. INTRODUCTION

TiO_2 is a widely employed material due to its important technological applications in photocatalytic and photoelectric devices, chemical sensors, and optical coatings.[1-4] TiO_2 presents three crystalline structures: brookite, anatase and rutile. The most common are anatase and rutile, since brookite is rather unstable. Submitting TiO_2 to high thermal treatments provokes the transformation of anatase to rutile, which is the thermodynamically stable phase at high temperatures. The different phases can affect several properties of titania, such as the catalytic activity or the gas sensing response.[5] Moreover, the titania grain size increases when anatase transforms to rutile, which alters the sensing response as well. The temperature at which the phase transition occurs depends on the preparation method, the precursors used, and the additives introduced in the base TiO_2.

Nanostructured materials have been widely investigated because they demonstrate wide functionality and exhibit enhanced or different properties compared to bulk materials.[6,7] Particularly, in the case of nanostructured ceramics, the presence of a large fraction of grain boundaries can lead to unusual or improved mechanical, electrical, optical, sensing, magnetic, and biomedical properties.[8-14]

When conventional sintering processes are used to sinter nano-sized titania powders, concomitant grain growth leads to the destruction of the nanostructure. This focuses attention on consolidation methods in which grain growth can be eliminated or significantly reduced. To accomplish this, rapid sintering methods have been widely used to sinter nano-sized powders. The most obvious advantage of rapid sintering is that fast heating and cooling rates, as well as short dwell time lead to bypassing low-temperature, non-densifying mass transport (e.g., surface diffusion).[15-17] However, conventional rapid heating can lead to temperature gradients and thus differential densification (non-uniform microstructures), low density, or specimen cracking. In order to overcome these difficulties, other rapid sintering techniques, such as the spark plasma sintering (SPS) method,[18-20] have been developed.

High-frequency induction heated sintering (HFIHS) is a new rapid sintering method, which was recently developed for the fabrication of ceramics and composites.[21,22] This method combines a short time and high-temperature exposure with a pressure application. During the HFIHS, a large current will be induced in the sample and in the graphite dye. As a result, the sample can be sintered both uniformly and rapidly. In this work, we report results on the sintering of rutile titanium oxide by the HFIHS method. The goal of this work is to produce dense, nanostructured TiO_2 ceramics in relatively short sintering times. In addition we report on the effect of high-energy ball milling in regards to the sintering behavior, the microstructure and the mechanical properties

*Corresponding author: ijshon@chonbuk.ac.kr

of the densified TiO_2 materials.

2. EXPERIMENTAL PROCEDURE

The anatase titanium oxide powder used in this research was supplied by Alfa, Inc.. The powder had a grain size of −325 mesh and was reported to be 99.6% pure. The powder was first milled in a high-energy ball mill (Pulverisette-5 planetary mill) at 250 rpm for various time periods (0, 1, 4, and 10 h). Tungsten carbide balls (9 mm in diameter) were used in a sealed cylindrical stainless steel vial under an argon atmosphere. The weight ratio of balls-to-powder was 30:1. Milling resulted in a significant reduction of the particle size. The crystallite size of TiO_2 powders was calculated from the full width at half-maximum (FWHM) of the diffraction peak by Suryanarayana and Grant Norton's formula:[23]

$$B_r\,(B_{crystalline} + B_{strain})\cos\theta = k\lambda / L + \eta\sin\theta \quad (1)$$

where B_r is the full width at half-maximum (FWHM) of the diffraction peak after instrumental correction; $B_{crystalline}$ and B_{strain} are FWHM caused by small grain size and internal stress, respectively; k is a constant (with a value of 0.9); λ is wavelength of the x-ray radiation; L and η are the grain size and internal strain, respectively; and θ is the Bragg angle. The parameters B and B_r follow Cauchy's form with the relationship: $B = B_r + B_s$, where B and B_s are the FWHM of the broadened Bragg peaks and the standard sample's Bragg peaks, respectively.

The TiO_2 powders were placed in a graphite dye (outside diameter, 35 mm; inside diameter, 10 mm; height, 40 mm) and then introduced into the high-frequency induction-heated sintering system (Eltek Co., Korea). A schematic diagram of this method is shown in Fig. 1. The system was first evacuated and a uniaxial pressure of 80 MPa was applied. An induced current (frequency of about 50 kHz) was then activated and maintained until the densification rate was negligible, indicated by the observed shrinkage of the sample. Sample shrinkage is measured in real time by a linear gauge measuring the vertical displacement. Temperatures were measured by a pyrometer focused on the surface of the graphite dye. At the end of the process, the induced current was turned off and the sample was allowed to cool to room temperature. The process was carried out under a vacuum of 40 mtorr (5.33 Pa).

The relative density of the sintered sample was measured by the Archimedes method. Microstructural information was obtained from product samples, which had been polished and etched using thermal etching for 1 h at 750°C. Compositional and microstructural analyses of the products were conducted through x-ray diffraction (XRD) and a field emission scanning electron microscope (FE-SEM) with energy dispersive spectroscopy (EDS). Vickers hardness was measured by performing indentations at a load of 10 kg and a dwell time of 15 s.

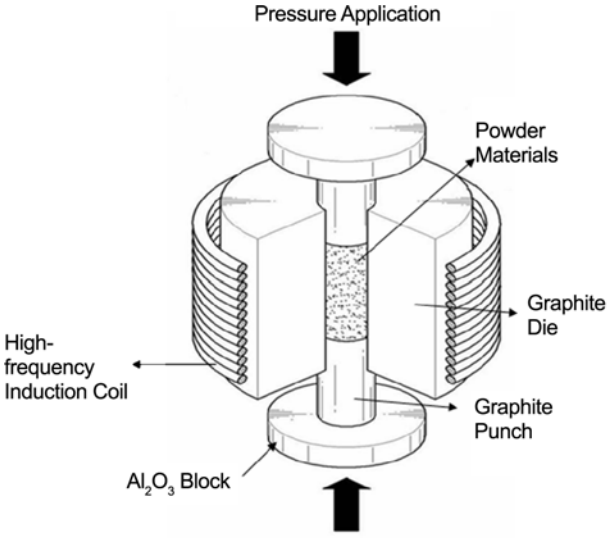

Fig. 1. Schematic diagram of the apparatus for high-frequency induction heated sintering (HFIHS).

3. RESULTS AND DISCUSSION

High-energy milling refined the microstructure of TiO_2 particles. Figure 2(a-d) shows x-ray diffraction patterns of the TiO_2 powders after milling for 1 - 10 hrs. The broadening of TiO_2 peaks due to crystallite refinement is evident after milling for 1 h, and it was continuously broadened during prolonged milling. The milling process is known to introduce impurities from the ball and/or container. However, in this study, peaks other than TiO_2 were not identified. To calculate the size of TiO_2 crystallite, the plot of $B\cos\theta$ versus $\sin\theta$ for TiO_2 with various milled powders is shown in Fig. 3. The TiO_2 crystallite size produced by Suryanarayana and Grant Norton's formula was reduced to 70, 31, and 20 nm by milling for 1, 4, 10 h, respectively. The reduction in the size of crystallite was most pronounced during the 1st hour of milling.

Figure 4 illustrates the shrinkage record of TiO_2 compacts under the applied pressure of 80 MPa. In all cases, there was a brief period of thermal expansion as soon as the induced current was applied. After the initial expansion, the shrinkage displacement increases with heating time and the onset of continuous shrinkage depends on the milling conditions. The amount of shrinkage displacement, which should be an indication of the degree of densification, increases with the milling time. It is clearly seen that the shrinkage-start temperature decreases as the milling time increases. The as-received TiO_2 powders began to shrink after approximately 20 sec, which corresponds to 640°C. In contrast, TiO_2 powders milled for 10 h start to shrink at a much lower tempera-

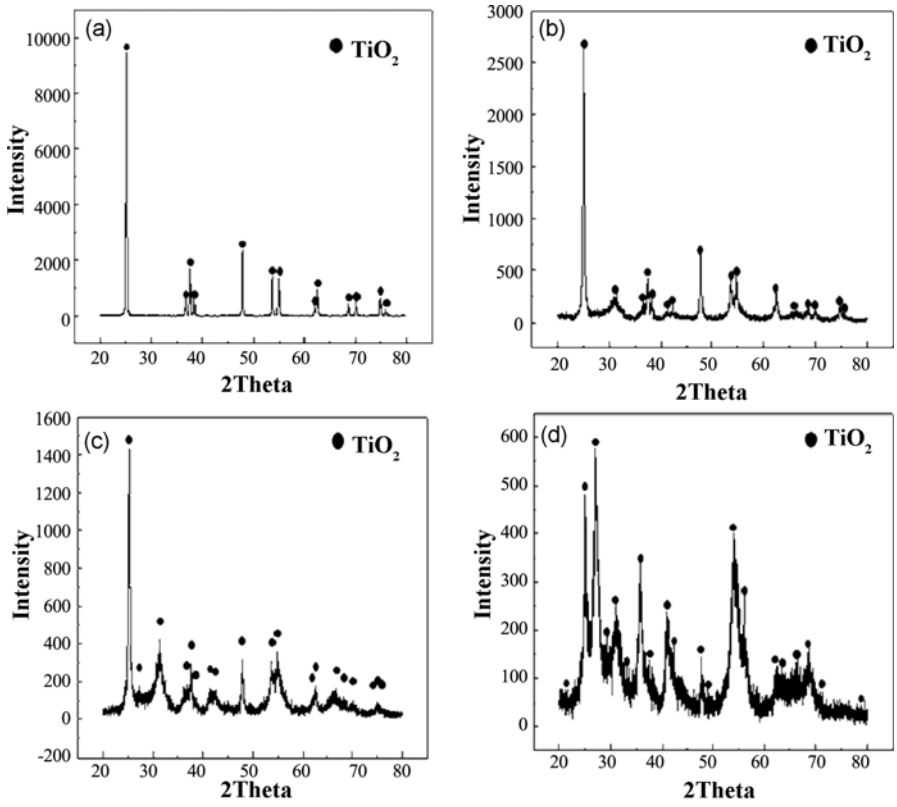

Fig. 2. X-ray diffraction patterns of the TiO_2 powders after high-energy milling for various durations: (a) as-received (b) milled for 1 h, (c) milled for 4 h, and (d) milled for 10 h.

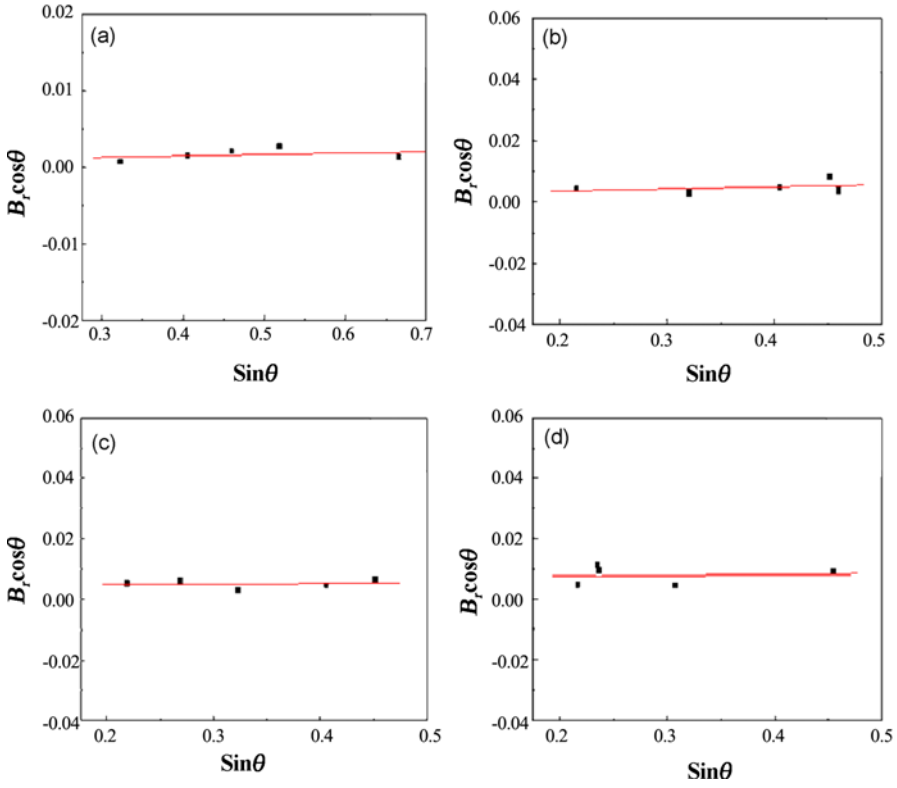

Fig. 3. Plot of Brcosθ versus sinθ for TiO_2 powders after milling for various durations: (a) as received, (b) 1 h, (c) 4 h, and (d) 10 h.

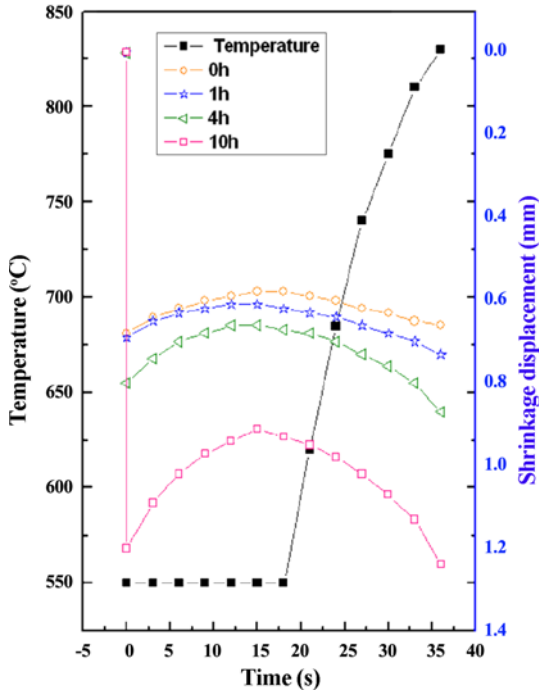

Fig. 4. Shrinkage displacement-temperature curve during the high-frequency induction heated sintering of TiO_2 powders milled for various durations.

ture. This demonstrates the effectiveness of prior-milling on the densification of TiO_2 powders. A high-energy ball milling treatment allows for the control of the formation of the compound by fixing the reactant powder microstructure. Indeed, high-energy ball milling produces finer crystallites, more strain and defects. Therefore, the consolidation temperature decreases with milling time because the driving force for sintering and the contact points of powders for atomic diffusion increases.

Figure 5 shows the x-ray diffraction patterns of TiO_2 sintered from various milled powders. All peaks are TiO_2 and their peak broadening was seen to reduce suggesting that there would be some grain growth during sintering. Figure 6(a-d) shows SEM images for the polished surface of the sintered TiO_2 compact. The reduction of pore volume with milling time is obvious. It became dense and had a more refined microstructure as the milling time increased. Figure 7 shows the effect of milling on the crystallite size and relative density for sintered compacts. The crystallite size is seen to decrease significantly by milling and the relative density increases by milling. The increase in size of the crystallite during sintering suggests that some grain growth occurred. Nevertheless, the average crystallite size of the sintered TiO_2 is not much larger than that of the milled powders and is still

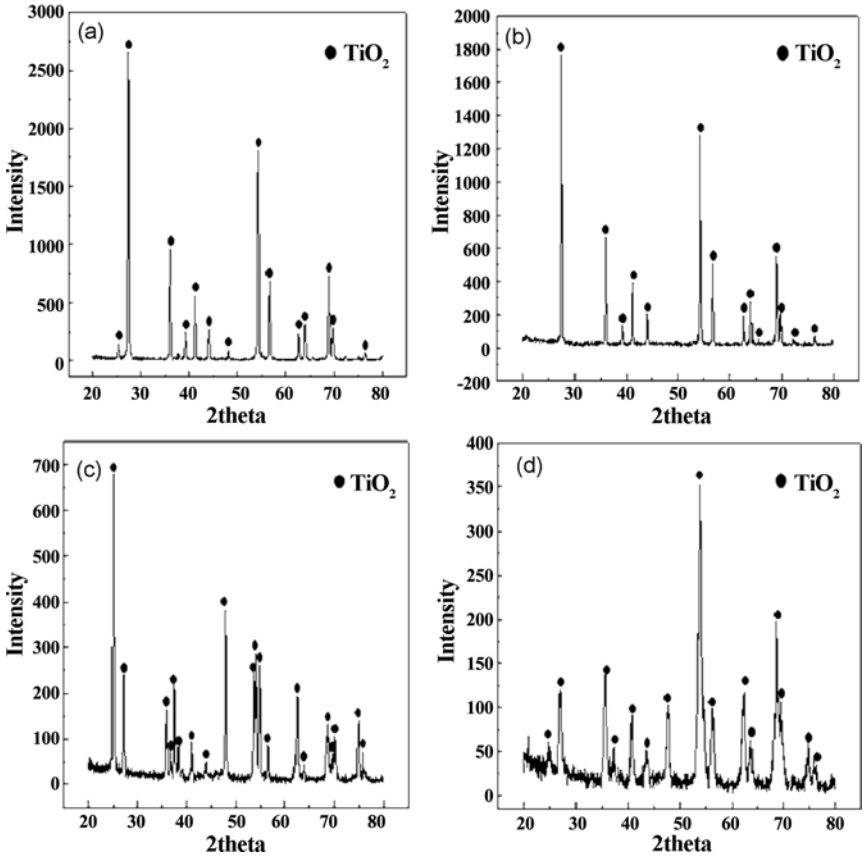

Fig. 5. X-ray diffraction patterns of the sintered compact using TiO_2 powders after milling for various durations: (a) as-received, (b) milled for 1 h, (c) milled for 4 h, and (d) milled for 10 h.

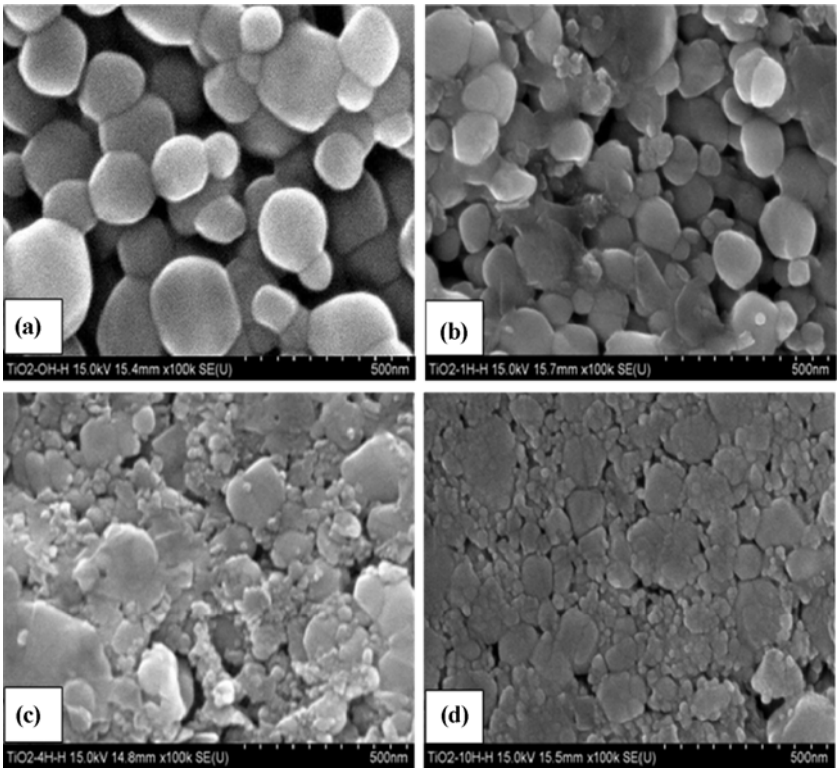

Fig. 6. FE-SEM micrographs showing the polished and etched surface of TiO_2 compacts: (a) as-received, (b) milled for 1 h, (c) milled for 4 h, and (d) milled for 10 h.

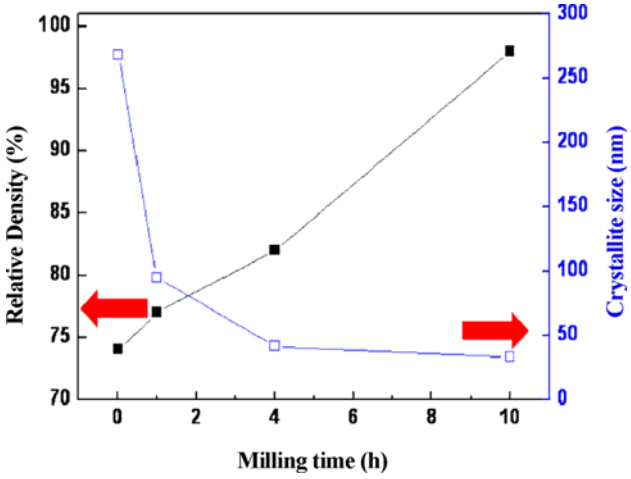

Fig. 7. Variation of relative density and grain size of TiO_2 sintered from various milled powders.

in the nano-scale realm. The retention of the nanoscale crystallite size might be attributed to the high heating rate and the relatively short exposure time of the powders to high temperature in HFIHS. The role of the current (resistive or inductive) in sintering has been the focus of several attempts aimed at providing an explanation regarding the observed enhancement of sintering and the improved characteristics of the products. The role played by the current has been variously interpreted, the effect being explained in terms of a fast heating rate due to Joule heating, the presence of a plasma in pores separating powder particles, and the intrinsic contribution of the current to mass transport.[24-27]

Vickers hardness and fracture toughness was measured to evaluate the mechanical properties of TiO_2 compact. Vickers hardness measurements were performed on polished sections of the TiO_2 samples using a 10 kg_f load and 15 s dwell time. Indentations with large enough loads produced radial cracks emanating from the corners of the indent. The lengths of these cracks permit estimation for the fracture toughness of the materials by means of the expression:[28]

$$K_{IC} = 0.203(c/a)^{-3/2} \cdot H_v \cdot a^{1/2} \quad (2)$$

where c is the trace length of the crack measured from the center of the indentation, a is one half of the average length for the two indent diagonals, and H_v is the hardness.

Figure 8 demonstrates the hardness and fracture toughness of TiO_2 sintered from various milled powders. The hardness and fracture toughness increased as the milling time increased. This effect may be attributed to the refined microstructure and/or higher density. A higher magnification view of the indentation median crack in a TiO_2 sample sintered from milled powder for 10 h is shown in Fig. 9(b), which shows that the crack propagated deflectively (↑).

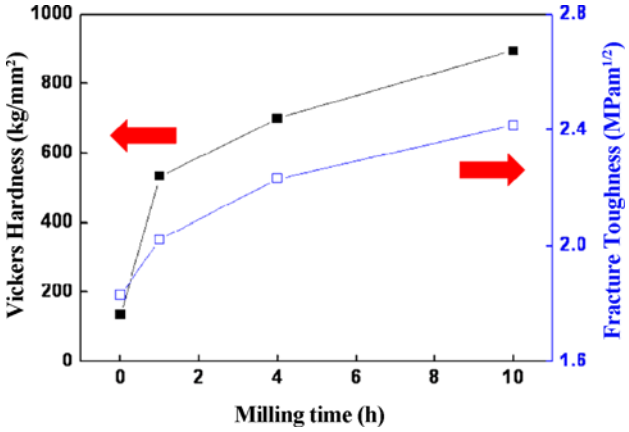

Fig. 8. Variation of hardness and fracture toughness of TiO_2 sintered from various milled powders.

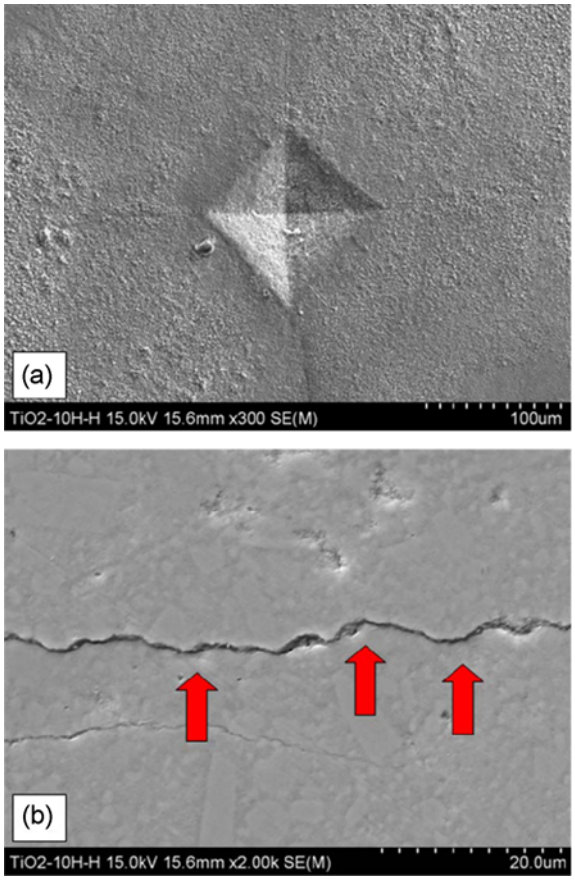

Fig. 9. (a) Vickers hardness indentation and (b) median crack propagating of TiO_2 sintered from milled powder for 10 h.

4. CONCLUSIONS

Commercial TiO_2 powders were high-energy ball milled for various durations and consolidated using the high-frequency induction heated sintering method (HFIHS). The ball milling substantially refined the crystallite structure of TiO_2 powders and facilitated the subsequent densification process. The consolidation temperature of TiO_2 powders was reduced by milling. Milling for 10 h reduced the crystallite size from 206 nm to 20 nm. The rapid consolidation of the HFIHS process retained the nanostructure after sintering. The microhardness and fracture toughness of sintered TiO_2 increased as the milling time increased. This effect may be attributed to the refined microstructure and/or higher density.

ACKNOWLEGEMENTS

This work is partially supported by KIST Future Resource Research Program and by the Human Resources Development of the Korea Institute of Energy Technology Evaluation and Planning (KETEP) grant funded by the Korea government Ministry of Knowledge Economy (No. 20114030200060).

REFERENCES

1. K. Iketani, R. D. Sun, M. Toki, K. Hirota, and O. Yamaguchi, *J. Phys. Chem. Solids* **64**, 507 (2003).
2. C. J. Barbé, F. Arendse, P. Comte, M. Jirousek, F. Lenzmann, V. Shklover, and M. Grätzel, *J. Am. Ceram. Soc*. **80**, 3157 (1997).
3. C. Garzella, E. Comini, E. Bontempi, L. E. Depero, C. Frigeri, and G. Sberveglieri, *Sens. Actuators B* **83**, 230 (2002).
4. D. J. Kim, S. H. Hahn, S. H. Oh, and E. J. Kim, *Mater. Lett*. **57**, 355 (2002).
5. D. Qin, W. Chang, J. Zhou, and Y. Chen, *Thermochim. Acta* **236**, 205 (1994).
6. H. Gleiter, *Nanostructured Materials* **6**, 3 (1995).
7. J. R. Yoon, D. J. Choi, K. H. Lee, J. Y. Lee, and Y. H. Kim, *Electron. Mater. Lett*. **4**, 167 (2008).
8. J. Karch, R. Birringer, and H. Gleiter, *Nature* **330**, 556 (1987).
9. A. M. George, J. Iniguez, and L. Bellaiche, *Nature* **413**, 54 (2001).
10. T. Prakash, *Electron. Mater. Lett.* **8**, 231 (2012).
11. C. Xu, J. Tamaki, N. Miura, and N. Yamazoe, *Sensors and Actuators B: Chemical.* **3**, 147 (1991).
12. D. G. Lamas, A. Caneiro, D. Niebieskikwiat, R. D. Sanchez, D. Garcia, and B. Alascio, *Journal of Magnetism and Magnetic Materials.* **241**, 207 (2002).
13. C. W. Nahm, C. J. Kim, Y. J. Park, B. J. Lee, and B. W. Park, *Electron. Mater. Lett.* **4**, 5 (2008).
14. E. S. Ahn, N. J. Gleason, A. Nakahira, and J. Y. Ying, *Nano Lett.* **1**, 149 (2001).
15. A. Morell and A. Mermosin, *Bull. Am. Ceram. Soc*. **59**, 626 (1980).
16. D. J. Chen and M. J. Mayo, *J. Am. Ceram. Soc.* **79**, 906 (1996).
17. D. J. Chen and M. J. Mayo, *NanoStruct. Mater.* **2**, 469 (1993).

18. I. J. Shon, S. L. Du, I. Y. Ko, J. M. Doh, J. K. Yoon, and J. H. Park, *Electron. Mater. Lett.* **7**, 133 (2011).
19. H.-S. Kang, I.-Y. Ko, J.-K. Yoon, J.-M. Doh, K.-T. Hong, and I.-J. Shon, *Met. Mater. Int.* **17**, 57 (2011).
20. I.-J. Shon, H.-Y. Song, S.-W. Cho, W. B. Kim, and C.-Y. Suh, *Korean J. Met. Mater.* **50**, 39 (2012).
21. N. R. Park, I. Y. Ko, J. K. Yoon, J. M. Doh, and I. J. Shon, *Met. Mater. Int*. **17**, 233 (2011).
22. S. L. Du, S. H. Cho, I. Y. Ko, J. M. Doh, J. K. Yoon, S. W. Park, and I. J. Shon, *Korean J. Met. Mater.* **49**, 231 (2011).
23. C. Suryanarayana and M. Grant Norton, *X-ray Diffraction A Practical Approach*, p. 207, Plenum Press, New York (1998).
24. Z. Shen, M. Johnsson, Z. Zhao, and M. Nygren, *J. Am. Ceram. Soc.* **85**, 1921 (2002).
25. J. E. Garay, U. Anselmi-Tamburini, Z. A. Munir, S. C. Glade, and P. Asoka-Kumar, *Appl. Phys. Lett.* **85**, 573 (2004).
26. J. R. Friedman, J. E. Garay, U. Anselmi-Tamburini, and Z. A. Munir, *Intermetallics* **12**, 589 (2004).
27. J. E. Garay, U. Anselmi-Tamburini, and Z. A. Munir, *Acta. Mater.* **51**, 4487 (2003).
28. K. Niihara, R. Morena, and D. P. H. Hasselman, *J. Mater. Sci. Lett*. **1**, 12 (1982).